Research Article Vol. 37, No. 11 / November 2020 / Journal of the Optical Society of America B 3335

Journal of the Optical Society of America B

OPTICAL PHYSICS

Giant resonant enhancement of optical binding of dielectric disks

E. N. Bulgakov,[1,2] K. N. Pichugin,[1] and A. F. Sadreev[1,*]

[1]Kirensky Institute of Physics, Federal Research Center KSC SB RAS, 660036 Krasnoyarsk, Russia
[2]Reshetnev Siberian State University of Science and Technology, 660037 Krasnoyarsk, Russia
*Corresponding author: almas@tnp.krasn.ru

Received 14 July 2020; revised 28 August 2020; accepted 28 August 2020; posted 15 September 2020 (Doc. ID 402659); published 19 October 2020

Two-fold variation over the aspect ratio of each disk and distance between disks gives rise to numerous events of avoided crossing of resonances of individual disks. For these events, the hybridized anti-bonding resonant modes can acquire a morphology close to the Mie resonant mode with the high orbital momentum of an equivalent sphere. The Q factor of such resonance can exceed the Q factor of an isolated disk by two orders of magnitude. We show that dual incoherent counterpropagating coaxial Bessel beams with power 1 mW/μm^2 with frequency resonant to such anti-bonding Mie-like modes result in unprecedented optical binding forces up to tens of nano-Newtons for silicon micrometer-sized disks. We show also that the magnitude and sign of optical forces depend strongly on the longitudinal wave vector of the Bessel beams.

https://doi.org/10.1364/JOSAB.402659

1. INTRODUCTION

The response of a microscopic dielectric object to a light field can profoundly affect its motion. A classic example of this influence is an optical trap, which can hold a particle in a tightly focused light beam [1]. When two or more particles are present, the multiple scattering between the objects can, under certain conditions, lead to optically bound states. This peculiar manifestation of optical forces is often referred to as optical binding (OB), and it was first discovered by Burns *et al.* on a system of two plastic spheres in water in 1989 [2]. Depending on the particle separation, OB leads to attractive or repulsive forces between the particles and, thus, contributes to the formation of stable configurations of particles. The phenomenon of OB can be realized, for example, in dual incoherent counterpropagating beam configurations [3–9]. Many researchers have analyzed OB force quantitatively in theory. Chaumet *et al.* [10] and Ng *et al.* [11] calculated the OB force under illumination of two counterpropagating plane waves. Čižmár *et al.* [12] presented the first theoretical and experimental study of dielectric sub-micrometer particle behavior and their binding in an optical field generated by interference of two counterpropagating Bessel beams.

An excitation of the resonant modes with a high Q factor in dielectric structures results in large enhancement of near electromagnetic (EM) fields and, respectively, in extremely large EM forces proportional to squared EM fields. First, sharp features in the force spectrum, causing mutual attraction or repulsion between successive photonic crystal layers of dielectric spheres under illumination of a plane wave, were revealed by Antonoyiannakis and Pendry [13]. Because of the periodicity of the structure, each layer is specified by extremely narrow resonances that transform into sharp resonant bonding and anti-boding resonances for a close approach of the layers. Also, it was revealed that the lower frequency bonding resonance forces act to push the two layers together and the higher frequency anti-bonding resonance to pull them apart. Later these disclosures we reported for coupled photonic crystal slabs [14], for coupled asymmetric membranes [15], and two planar dielectric photonic metamaterials [16] due to the existence of resonant states with infinite Q factors (bound states in the continuum).

Even two particles can demonstrate precedents of extremely high Q factor resonant modes owing to the mechanism of avoided crossing. A good example is the avoided crossing of whispering-gallery modes (WGMs) in coupled microdisks [17], which resulted in extremely high enhancement of OB between coupled WGM spherical resonators [18]. However, the WGM modes can be excited only in spheres with large radii of order 30 μm. Respectively, the OB force for such massive particles can turn out to be not so significant. In the present paper, we offer a solution to the problem by use of two coaxial silicon disks of micrometer sizes, shown in Fig. 1, whose resonant modes can have extremely high Q factors in the subwavelength regime. Owing to two-fold (over the aspect ratio and distance between disks) avoided crossing of low-order resonances, the anti-bonding resonant mode acquires a morphology of the high-order Mie resonant mode of an effective larger sphere with extremely small radiation losses [19]. We show also that the

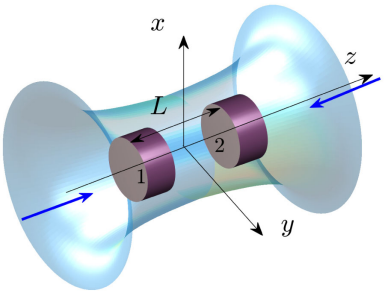

Fig. 1. Two silicon disks with radius a, thickness h, and permittivity $\epsilon = 12$ are illuminated by dual counterpropagating mutually incoherent Bessel beams with zero azimuthal index $m = 0$. Light intensity of each beam 1 mW/μm^2.

magnitude and, more interestingly, the sign of the OB force depend strongly on the wave numbers of the Bessel beams, which opens additional options to manipulate high index particles optically.

2. TWO-FOLD AVOIDED CROSSING OF RESONANCES

The phenomenon of avoided resonance crossing has attracted interest in photonics by enhancement of the Q factor of resonant modes in coupled optical microcavities in the WGM regime [20,21]. Interest was renewed when high Q resonant modes were revealed even in isolated dielectric disks showing high Q factors, owing to the avoided crossing of resonant modes for variation of the aspect ratio in *subwavelength* range [22]. Because of the importance of this result, we reproduce that process in Fig. 2(a). All 2D calculations were performed based on the aperiodic-Fourier modal method [23], complemented by COMSOL numerics. Throughout the paper, the radii of disks are fixed at $a = 0.5$ μm. At the aspect ratio $a/h = 0.71$, the Q factor reaches maximal value around 160 for high index optical material (Si), as shown in Fig. 2(b). One can see that the hybridized mode has a morphology very close to the morphology of the Mie resonant mode with orbital momentum $l = 3$ in an equivalent sphere whose volume equals $\pi a^2 h$. This Mie mode and equivalent sphere are highlighted by a white circle in the upper inset of Fig. 2(a). The spherical particle has a minimal surface compared to the given volume and therefore the smallest radiation losses compared to particles with other shapes. That explains the peak in the Q factor of the corresponding resonant mode in Fig. 2(b). The multipole conversion from lower to higher orders of the multipole modes gives an alternative explanation of minimization of radiation losses [19,24,25].

If this optimal aspect ratio is fixed at $a/h = 0.71$ and traverses over the distance between disks, the Q factor is enhanced by a few times compared to the isolated disk [26]. Evolution of the resonances and the behavior of the Q factor $Q = -\frac{\mathrm{Re}(ka)}{2\mathrm{Im}(ka)}$ are shown in Figs. 2(c) and 2(d), respectively. At $L \gg a$, the resonances are degenerate, marked by a cross in Fig. 2(c). For an approach of disks, the resonances are split and evolve spirally so that at some distances, the imaginary parts of hybridized complex resonant frequencies reach some minima, marked in Fig. 2(c) by closed circles. The spiral behavior of complex

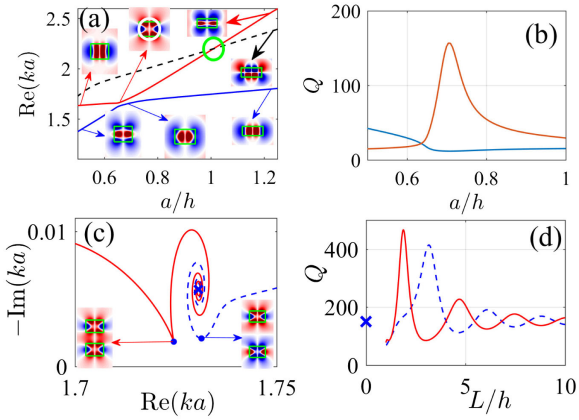

Fig. 2. (a) Avoided crossing of two TE resonances whose modes are symmetric relative to $z \to -z$ and (b) their Q factors versus the aspect ratio a/h in isolated silicon disk with dielectric constant $\epsilon = 12$. Insets show the profiles of tangential component of electric field E_ϕ. Crosses mark the degenerate resonant frequencies and, respectively, the Q factor of isolated disks. (c), (d) Evolution of resonances and the Q factor versus distance between disks at $a/h = 0.71$.

resonant frequencies is a result of radiation of leaky resonant modes by one disk and consequent scattering by the other. These scattering processes give rise to the coupling e^{ikL}/L^2 that hybridizes the resonant modes of separate disks as leaky bonding and anti-bonding resonant modes [26]. They are shown in insets in Fig. 2(c) at left (bonding mode) and right (anti-bonding mode) at distances at which the Q factor reaches the maxima, $L/h = 1.87$ and $L/h = 3.16$, respectively, as shown in Fig. 2(d).

3. OPTICAL BINDING FORCES

It is clear that the same mechanism of consequent scattering processes underlies OB and, respectively, the OB force stimulated by incident Bessel beams. It is reasonable to consider the OB force of disks with optimized aspect ratio $a/h = 0.71$ at distances at which the bonding and anti-bonding resonant modes show maximal Q factors. We consider the Bessel beams with TE polarization in the simplest form with zero azimuthal index $m = 0$ [27]:

$$\mathbf{E}_{\mathrm{inc}}(r, \phi, z) = E_0 \mathbf{e}_\phi \exp(\pm i k_z z) J_1(k_r r), \tag{1}$$

where J_1 is the Bessel function, k_z and k_r are the longitudinal and transverse wave numbers, respectively, with frequency $\omega/c = k = \sqrt{k_r^2 + k_z^2}$, r, ϕ, and z are the cylindrical coordinates, and $\mathbf{e}_\phi$ is the unit vector of the polarization. The total system of two disks and applied Bessel beams preserves the axial symmetry, which allows us to consider the simplest case with zero azimuthal index $m = 0$. In order to stabilize both disks in z direction, we use the approach in which two counterpropagating mutually incoherent Bessel beams are applied [3,5], which is schematically shown in Fig. 1. This allows to neglect interference between beams and calculate separately the forces on each disk defined by only the intensity of left/right beams.

Next, we considered the transverse stability of a single disk at $r = 0$. Numerical calculations of differences between forces

produced by the centered Bessel beam and the force produced by a slightly shifted beam show that the Bessel beams strongly trap disks at the symmetry axis, i.e., at $r = 0$ (stable zero-force points), similar to the case of a sphere [28]. Finally, there is the problem of angular stability relative to rotation of the disks. That problem was considered recently by Seberson and Robicheaux [29] who showed the high angular stability of a single disk in a Gaussian standing wave. The two counter-propagating Bessel beams (1) do not carry angular momentum and therefore are very similar to the Gaussian standing beam. Therefore, we can assume that there is also angular stability. This considerably simplifies the further calculation of the OB force between two disks and allows to consider the optical forces over the axis of symmetry only. We define the OB force $F_{\rm OB}^{\rightarrow} = (F_{1z} - F_{2z})/2$, where the indices 1 and 2 note the disks where the Bessel beam is incident at the left. Owing to the incoherence of the Bessel beam illuminated from the right, we have the same expression for $F_{\rm OB}^{\leftarrow} = -F_{\rm OB}^{\rightarrow}$. As a result, we obtain a doubled value for the OB force $F_{\rm OB} = F_{1z} - F_{2z}$ and zero optical pressure on both disks. The results of numerical calculations are presented in Fig. 3, where we can see that the OB force is sensitive to the resonant frequencies shown by green solid (bonding) and dashed (anti-bonding) lines. One can see that the bonding and anti-bonding resonances shown in Fig. 2 that achieve a Q factor above 400 have no significant bright effect on the OB force, as Fig. 3 shows. We see that the maximal OB force is enhanced by three orders and reaches a value of up to 1 nano-Newton.

Next, we show in Fig. 2(a) that the antisymmetric resonance (black dashed line) crosses the symmetric resonance (red solid line) at $a/h = 1.009$. These resonances are not coupled in the isolated disk because of their orthogonality to each other. However, as soon as the second disk approaches this symmetry, prohibition is removed. Evolution of these resonances with distance L between disks is shown in Fig. 4. When the distance is large enough, the resonances marked by green crosses are degenerate. Let us define the corresponding modes as $\psi_1(\vec{r})$ and $\psi_2(\vec{r})$, which are shown in Fig. 4 in the upper insets at $L = \infty$. With the approaching of the disks, these resonant

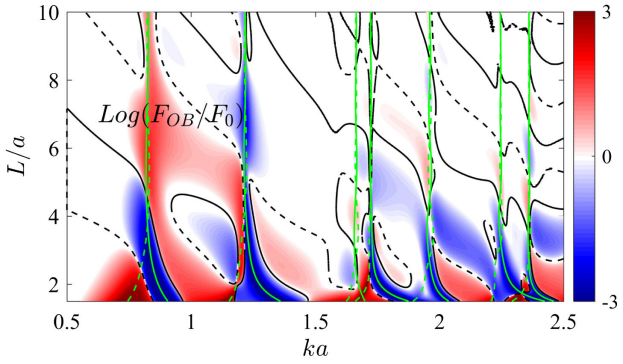

Fig. 3. OB force between two disks versus the frequency and distance between centers of disks with radius $a = 0.5$ μm, aspect ratio $a/h = 0.71$, and $\epsilon = 12$ under illumination of the Bessel beam with TE polarization and $k_z a = 1$. Black solid (dashed) lines show stable (unstable) distances between disks. Green solid (dashed) lines show anti-bonding (anti-symmetric) and bonding (symmetric) resonant frequencies of two disks versus the distance between. $F_0 = 1$ pN.

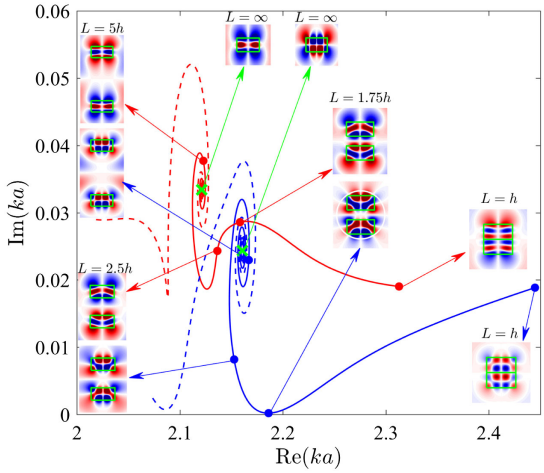

Fig. 4. Avoided crossing of resonances originated from coupling of orthogonal resonances of isolated disk shown in Fig. 2(a) for variation of distance between disks for $a = 0.5$ μm, $a/h = 0.96$. Solid (dashed) lines show anti-bonding (bonding) resonances. Insets show the profiles of tangential component of electric field E_ϕ.

modes hybridize as follows [26]:

$$\psi_{1,2;s,a}(\vec{r}) \approx \psi_{1,2}\left(\vec{r}_\perp, z - \frac{1}{2}L\vec{z}\right) \pm \psi_{1,2}\left(\vec{r}_\perp, z + \frac{1}{2}L\vec{z}\right), \tag{2}$$

where $\vec{z}$ is the unit vector along the z axis. These modes can be classified as bonding (symmetrical) or anti-bonding (anti-symmetrical) resonant modes and are illustrated in Fig. 4 at $L = 5a$. However, with a further approaching of the disks, the approximation (2) ceases to be correct because of the interaction of the resonances ψ_1 and ψ_2. One can observe noticeable deformation of these resonant modes at $L/h = 2.5$ in Fig. 4 and especially at $L/h = 1.68$. At this distance and the aspect ratio $a/h = 0.96$, the anti-bonding resonant mode highlighted in Fig. 4 by an open circle features an extremely low resonant width, as marked by a closed circle. Respectively, one can observe an extremely high peak of the Q factor around 5500 in Fig. 5 at the vicinity of points $L/h = 1.68$ and $a/h = 0.96$. The further approach of disks until they touch each other at $L = h$ results in resonant modes surprisingly close to approximation (2), as the insets in the right side of Fig. 4 show. The reason for extremely small radiation losses of the anti-bonding mode at the point of maximal Q factor is related to its morphology, which is immensely close to the morphology of the Mie resonant mode with orbital momentum $l = 6$ of a sphere with volume $\pi(h + L)a^2$. That sphere is highlighted in the corresponding inset in Fig. 4 by an open white circle.

It is worthy to note that this case of extreme enhancement of the Q factor due to the avoided crossing of orthogonal resonant modes of isolated disks is not unique. Figure 6, for example, demonstrates another scenario of the avoided crossing for the approach of disks with aspect ratio $a/h = 1.17$, however for higher lying resonant modes. The right inset shows an anti-bonding resonant mode that demonstrates an unprecedented Q factor of 15,000 at $L/h = 1.4$. Similar to the case shown in Fig. 4, the reason is that the morphology of the anti-bonding

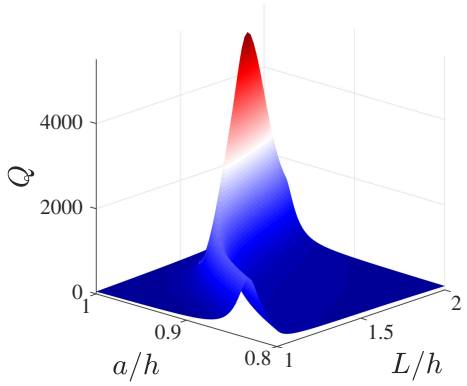

Fig. 5. Q factor versus aspect ratio and distance between disks of the anti-bonding resonant mode (blue line in Fig. 4 highlighted by open circle).

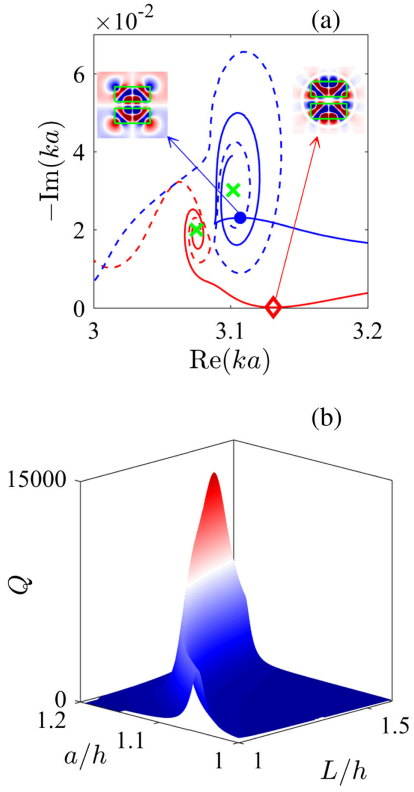

Fig. 6. (a) Evolution of the higher lying TE resonances in traversing with the distance between the disks for $a = 0.5$ μm, $a/h = 1.17$. Solid (dashed) lines show anti-bonding (bonding) resonances. (b) Q factor versus the distance between the disks and their aspect ratio.

resonant mode is close to the Mie resonant mode with $l = 8$, as highlighted by a white circle in the right inset in Fig. 6(a).

Figure 7 shows the OB force at $a/h = 0.96$ in log scale versus the frequency of the dual Bessel beams and distance L. In order for the reader to see the extreme behavior of the OB force, we reproduce the fragment highlighted by a black frame in Fig. 7 as the surface in Fig. 8(a), where one can see that giant OB is achieved at around 8 nano-Newtons at $ka = 2.19$, $L/h = 1.68$, $a/h = 0.96$, $k_z a = 0.5$. Figure 8(b) shows that this giant peak is

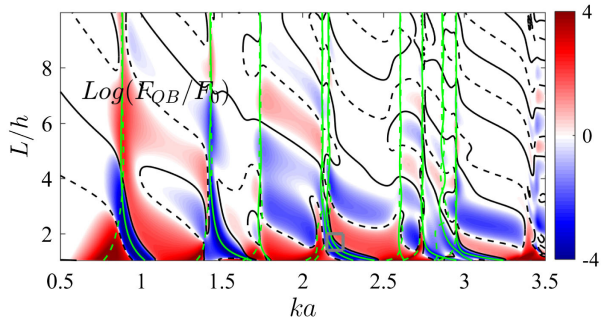

Fig. 7. Binding force between two disks versus the frequency and distance between centers of disks with aspect ratio $a = 0.5$ μm, $a/h = 0.96$ for the Bessel beam with TE polarization $k_z a = 0.5$ for disks with $\epsilon = 12$ and radius $a = 0.5$ μm. $F_0 = 1$ pN.

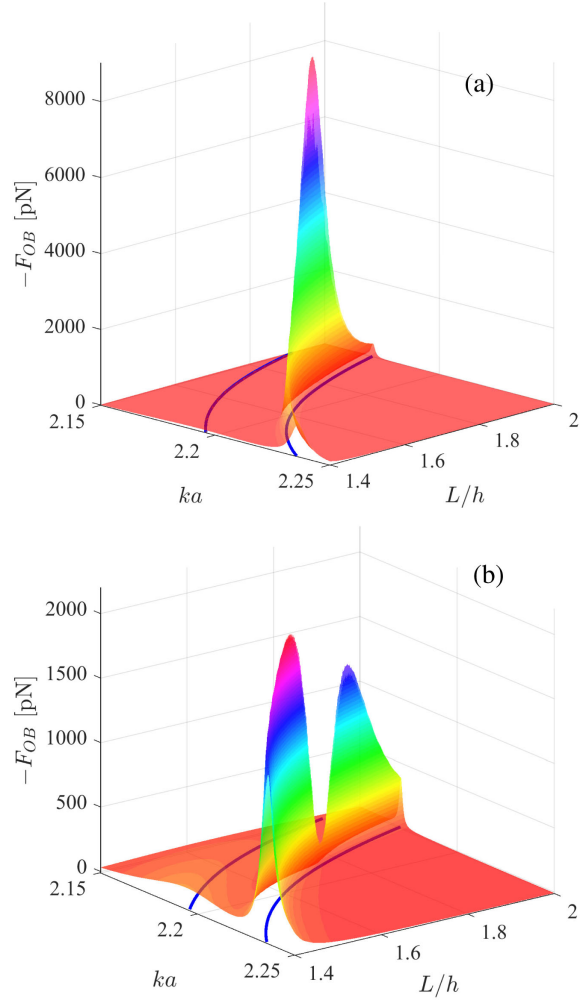

Fig. 8. OB versus distance between centers of disks at the vicinity of anti-bonding resonance highlighted by black frame in Fig. 7: (a) $k_z a = 0.5$ and (b) $k_z a = 1$. Solid lines underneath show bonding and anti-bonding resonant frequencies versus distance L/h shown in Fig. 7 by green lines.

split for $k_z a = 1$. It is remarkable that the equilibrium distances between disks is traversed close to the anti-bonding resonance shown by a solid line.

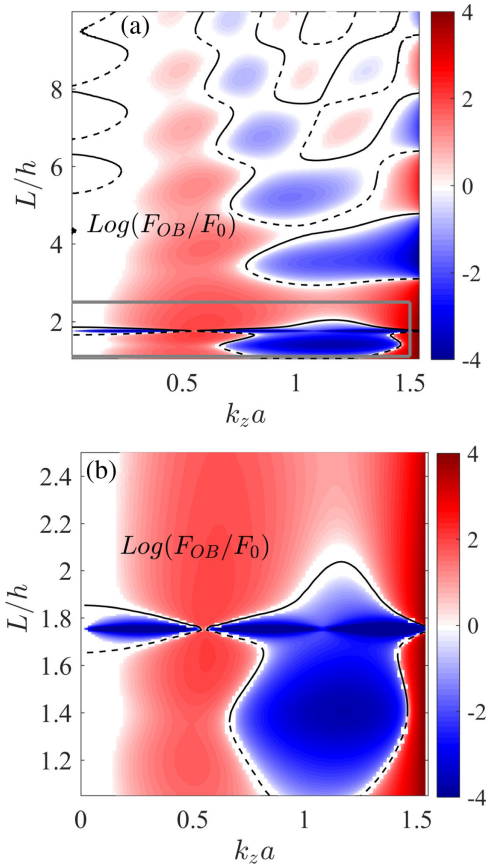

Fig. 9. (a) OB force versus distance between disks and longitudinal wave vector of the Bessel beam $k_z a$ at the vicinity of anti-bonding resonance marked in Fig. 4(b) by open circle $ka = 2.19$, $a/h = 0.96$, $a = 0.5$ μm. (b) Zoomed version of (a). Black solid (dashed) lines show stable (unstable) distances between disks. $F_0 = 1$ pN.

Also, Fig. 8 shows that the OB forces depend crucially on the waist of the Bessel beams controlled by the longitudinal wave number k_z. Figure 9 shows that, first, the OB forces oscillate with distance and k_z, which is a result of mutual scattering by disks that bring the phase $e^{i2k_z L}$ [26]. However, this argument is applicable only when the distance between disks much exceeds the thickness of the disks. For distances closer, Fig. 9(a) shows an extremely large contribution of the bonding and anti-bonding resonances around $L/h = 1.75$. Moreover, one can see in the zoomed Fig. 9(b) the collapse of the OB forces at the point $L/h = 1.75$, $k_z a = 0.5$. Therefore, giant peaks in OB can be easily manipulated by small changes in parameters of the Bessel beam: $k_z a$ and frequency. The case of the Bessel beams resonant to the higher lying Mie-like resonant mode with $l = 8$ shown in Fig. 6(a) with the Q factor 15,000 gives the similar OB force shown in Fig. 7.

4. SUMMARY

In the present paper, we considered the resonant enhancement of the OB force of two silicon disks of micrometer size by illumination of dual incoherent counterpropagating Bessel beams. As distinct from the case of two dielectric spheres [10,11], the case of coaxial disks brings a new aspect for the OB force related to an extremely high Q factor due to the two-fold avoided crossing of orthogonal resonances over the aspect ratio and distance between the disks [19]. The corresponding anti-bonding resonant modes of two disks turn out to be close to the Mie resonant mode with high orbital index $l = 6$ or even $l = 8$ of an effective sphere with volume $4\pi R^3/3 = \pi(h + L)a^2$, which explains the extremely high Q factors. An alternative explanation is the multipole conversion from lower to higher orders of multipole modes [19,24,25]. For the case of two coaxial silicon disks with micrometer diameter illuminated by dual coaxial Bessel beams, we demonstrate a giant OB force in a few tens of nano-Newtons in the vicinity of anti-bonding resonances. Giant enhancement of optical forces has been reported already [13,14,16], however, for photonic crystal (PhC) layers and two layers in the waveguide [30]. It is remarkable that the OB force can be easily manipulated by counterpropagating Bessel beams. The OB force is extremely sensitive to frequency. Similar to the case of PhC layers, the lower frequency bonding resonance forces act to push the two disks together and the higher frequency anti-bonding resonance to pull them apart. However, for a fixed frequency, the sign of the OB force also depends on the waist of the Bessel beams.

Funding. Russian Science Support Foundation (19-02-00055).

Disclosures. The authors declare no conflicts of interest.

REFERENCES

1. A. Ashkin, J. M. Dziedzic, J. E. Bjorkholm, and S. Chu, "Observation of a single-beam gradient force dielectric particles," Opt. Lett. **11**, 288–292 (1986).
2. M. M. Burns, J.-M. Fournier, and J. A. Golovchenko, "Optical binding," Phys. Rev. Lett. **63**, 1233–1236 (1989).
3. S. A. Tatarkova, A. E. Carruthers, and K. Dholakia, "One-dimensional optically bound arrays of microscopic particles," Phys. Rev. Lett. **89**, 283901 (2002).
4. R. Gómez-Medina and J. J. Sáenz, "Unusually strong optical interactions between particles in quasi-one-dimensional geometries," Phys. Rev. Lett. **93**, 243602 (2004).
5. N. K. Metzger, K. Dholakia, and E. M. Wright, "Observation of bistability and hysteresis in optical binding of two dielectric spheres," Phys. Rev. Lett. **96**, 068102 (2006).
6. N. K. Metzger, E. M. Wright, and K. Dholakia, "Theory and simulation of the bistable behaviour of optically bound particles in the Mie size regime," New J. Phys. **8**, 139–153 (2006).
7. K. Dholakia and P. Zemánek, "Colloquium: gripped by light: optical binding," Rev. Mod. Phys. **82**, 1767–1791 (2010).
8. R. Bowman and M. Padgett, "Optical trapping and binding," Rep. Prog. Phys. **76**, 026401 (2013).
9. I. Thanopulos, D. Luckhaus, and R. Signorell, "Modeling of optical binding of submicron aerosol particles in counter propagating Bessel beams," Phys. Rev. A **95**, 063813 (2017).
10. P. C. Chaumet and M. Nieto-Vesperinas, "Optical binding of particles with or without the presence of a flat dielectric surface," Phys. Rev. B **64**, 035422 (2001).
11. J. Ng, Z. Lin, C. Chan, and P. Sheng, "Photonic clusters formed by dielectric microspheres: numerical simulations," Phys. Rev. B **72**, 085130 (2005).
12. T. Čižmár, V. Kollárová, Z. Bouchal, and P. Zemánek, "Sub-micron particle organization by self-imaging of non-diffracting beams," New J. Phys. **8**, 43–65 (2006).
13. M. I. Antonoyiannakis and J. B. Pendry, "Mie resonances and bonding in photonic crystals," Europhys. Lett. **40**, 613–618 (1997).

14. V. Liu, M. Povinelli, and S. Fan, "Resonance-enhanced optical forces between coupled photonic crystal slabs," Opt. Express **17**, 21897–21909 (2009).
15. A. Rodriguez, A. McCauley, P.-C. Hui, D. Woolf, E. Iwase, F. Capasso, M. Loncar, and S. Johnson, "Bonding, antibonding and tunable optical forces in asymmetric membranes," Opt. Express **19**, 2225–2241 (2011).
16. J. Zhang, K. MacDonald, and N. Zheludev, "Giant optical forces in planar dielectric photonic metamaterials," Opt. Lett. **39**, 4883–4886 (2014).
17. M. Benyoucef, J.-B. Shim, J. Wiersig, and O. G. Schmidt, "Quality-factor enhancement of supermodes in coupled microdisks," Opt. Lett. **36**, 1317–1319 (2011).
18. M. L. Povinelli, S. Johnson, M. Loncar, M. Ibanescu, E. Smythe, F. Capasso, and J. D. Joannopoulos, "High-Q enhancement of attractive and repulsive optical forces between coupled whispering-gallery-mode resonators," Opt. Express **13**, 8286–8295 (2005).
19. E. N. Bulgakov, K. N. Pichugin, and A. F. Sadreev, "Engineering of the extremely high-Q factor in two subwavelength dielectric resonators," arXiv:2005.05554 (2020).
20. J. Wiersig, "Formation of long-lived, scarlike modes near avoided resonance crossings in optical microcavities," Phys. Rev. Lett. **97**, 253901 (2006).
21. S. V. Boriskina, "Theoretical prediction of a dramatic Q-factor enhancement and degeneracy removal of whispering gallery modes in symmetrical photonic molecules," Opt. Lett. **31**, 338–340 (2006).
22. M. Rybin, K. Koshelev, Z. Sadrieva, K. Samusev, A. Bogdanov, M. Limonov, and Y. Kivshar, "High-Q supercavity modes in subwavelength dielectric resonators," Phys. Rev. Lett. **119**, 243901 (2017).
23. F. Bigourdan, J.-P. Hugonin, and P. Lalanne, "Aperiodic-Fourier modal method for analysis of body-of-revolution photonic structures," J. Opt. Soc. Am. A **31**, 1303–1311 (2014).
24. W. Chen, Y. Chen, and W. Liu, "Multipolar conversion induced subwavelength high-Q Kerker supermodes with unidirectional radiations," Laser Photon. Rev. **13**, 1900067 (2019).
25. Z. Sadrieva, K. Frizyuk, M. Petrov, Y. Kivshar, and A. Bogdanov, "Multipolar origin of bound states in the continuum," Phys. Rev. B **100**, 115303 (2019).
26. K. N. Pichugin and A. F. Sadreev, "Interaction between coaxial dielectric disks enhances the Q factor," J. Appl. Phys. **126**, 093105 (2019).
27. V. Karásek, O. Brzobohatý, and P. Zemánek, "Longitudinal optical binding of several spherical particles studied by the coupled dipole method," J. Opt. A **11**, 034009 (2009).
28. G. Milne, K. Dholakia, D. McGloin, K. Volke-Sepulveda, and P. Zemánek, "Transverse particle dynamics in a Bessel beam," Opt. Express **15**, 13972–13987 (2007).
29. T. Seberson and F. Robicheaux, "Stability and dynamics of optically levitated dielectric disks in a Gaussian standing wave beyond the harmonic approximation," arXiv:2006.07479 (2020).
30. A. F. Sadreev and E. Ya. Sherman, "Temporal oscillations of light transmission through dielectric nanoparticles subjected to optically induced motion," Phys. Rev. A **94**, 033820 (2016).